*31st EPS Conference on Plasma Phys. London, 28 June - 2 July 2004 ECA Vol.**28G**, P-5.105 (2004)*

Magnetic Island Generation in Nonlinear Evolution of Interchange Mode

K.Ichiguchi[1] , B.A.Carreras[2]

[1]*National Institute for Fusion Science, Oroshi-cho 322-6, Toki 509-5292, Japan*
[2]*Oak Ridge National Laboratory, Oak Ridge, Tennessee 37831, USA*[A]

Abstract : Generation of the magnetic islands in the nonlinear evolution of the resistive interchange mode is investigated numerically based on the reduced magnetohydrodynamics (MHD) equations. The islands are generated by the interchange flow of the instability without current concentration at the resonant surface. The deformation of the contour of the perturbed poloidal flux is essential in the island generation.

1. Introduction

In the linear analysis of the resistive interchange mode in the slab geometry, the mode structure of the poloidal magnetic flux is an odd function with respect to the resonant surface. Therefore, it is generally considered that magnetic islands are hardly generated by the interchange mode. On the other hand, significant magnetic islands were obtained in the nonlinear calculation of the interchange mode[1-3]. The common feature of these islands is that the number of the island in the poloidal cross section is twice of the poloidal mode number of the dominant component. This feature is quite different from that of the tearing mode. Thus, the mechanism of the island generation is discussed in the present paper.

2. Basic Equation and Configuration

The nonlinear evolution of the resistive interchange mode is examined by using the NORM code[3]. This code solves the reduced MHD equations for stream function Φ, poloidal flux Ψ and plasma pressure P. We employ the cylindrical geometry (r,θ,z) to avoid the stochasticity attributed to the toroidicity. In this case, the magnetic field $\mathbf{B}$ and the perpendicular velocity $\mathbf{v}_\perp$ are given by $\mathbf{B} = B_0\mathbf{e}_z + \mathbf{e}_z \times \nabla\Psi$ and $\mathbf{v}_\perp = \nabla\Phi \times \mathbf{e}_z$, respectively, where $\mathbf{e}_z$ denotes the unit vector in z direction.

In the present analysis, we employ the no net current equilibrium with the pressure profile of $P_{eq} = P_0(1-r^4)$ at $\beta_0 = 2\%$. The average curvature of the magnetic field line is calculated by using the cylindrical component of the LHD configuration, which drives the interchange mode with the pressure gradient. In this equilibrium, the rational surface with $\iota_{eq} = 1/2$ exists in the plasma column. Therefore, we investigate the perturbation with a single helicity of $n/m = 1/2$. Here, m and n denote the poloidal and the toroidal mode numbers, respectively. The perturbations are expanded in the Fourier series in the ways of $\tilde{\Psi} = \sum_n \tilde{\Psi}_{mn}(r)\cos(m\theta - n\zeta)$,

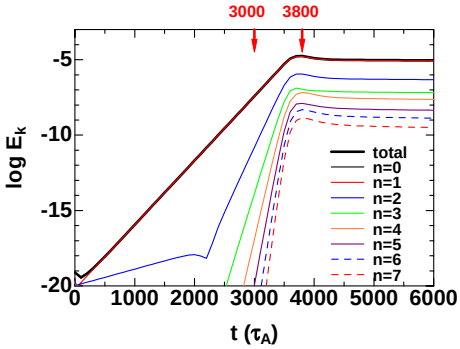

Fig.1. Time evolution of kinetic energy.

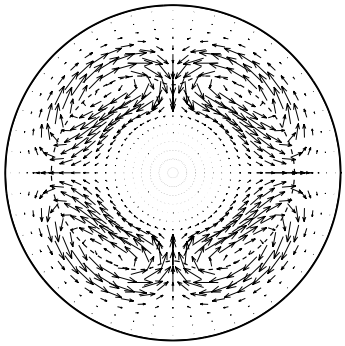

Fig.2. Flow pattern at $t = 3800\tau_A$ for $r \leq 0.8$.

$\tilde{\Phi} = \sum_n \tilde{\Phi}_{mn}(r)\sin(m\theta - n\zeta)$ and $\tilde{P} = \sum_n \tilde{P}_{mn}(r)\cos(m\theta - n\zeta)$, where $\zeta = z/R_0$. To clarify the reconnection process, we use a fairly large resistivity of $S = 10^4$, where S denotes the magnetic Reynolds number. The fluid viscosity and the perpendicular heat conductivity are introduced so that the $(m,n) = (2,1)$ component has the largest growth rate in the linear phase.

3. Island generation and reconnection mechanism

Figure 1 shows the time evolution of the kinetic energy, which is defined by $E_k = \sum_n E_k^n$, $E_k^n = \frac{1}{2}\int |\nabla_\perp \tilde{\Phi}_{mn}\sin(m\theta - n\zeta)|^2 dV$. The kinetic energy saturates at $t = 3700\tau_A$ and the $(m,n) = (2,1)$ mode is dominant in the whole time evolution, where τ_A denotes the poloidal Alfvén time. Figure 2 shows the flow pattern on the poloidal cross section of $z = 0$ at $t = 3800\tau_A$. We also plot the position of the resonant surface where the total rotational transform ι_T equals to 1/2, which is defined by $\iota_T(r,\theta,z) = \frac{1}{r}\frac{\partial}{\partial r}[\Psi_{eq}(r) + \tilde{\Psi}(r,\theta,z)]\frac{R_0}{B_0}$. Four vortices are seen around the resonant surface. This pattern corresponds to the typical linear eigenfunction of the interchange mode with $m = 2$. The surface with $\iota_T = 1/2$ is deformed by the radial component of the flow.

Since we treat the single helicity perturbation, the structure of the magnetic island can be observed by plotting the helical magnetic flux Ψ_h, which is defined by $\Psi_h(r,\theta,z) = \tilde{\Psi}(r,\theta,z) + \Psi_{eq}(r) - \frac{1}{2}r^2\frac{n}{m}\frac{B_0}{R_0}$. Figure 3 shows the contour of the helical flux on the poloidal cross section at $t = 3000\tau_A$ (linear phase) and $t = 3800\tau_A$ (nonlinear saturation phase). At $t = 3000\tau_A$, two thin islands are observed. The island structure is consistent with the linear eigenfunction of the $m = 2$ resistive interchange mode shown in Fig.4. In this case, $\tilde{\Psi}_{21}$ is an odd function with finite value at the resonant surface. These islands are considered to be generated spontaneously due to the cylindrical geometry and the large resistivity. The X-points of the spontaneous islands are maintained through the whole time evolution. We call them major X-points.

At $t = 3800\tau_A$, new X-points are generated at the positions of the O-points of the sponta-

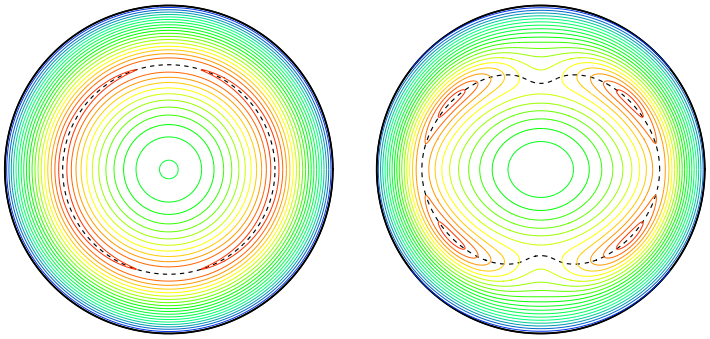

Fig.3. Contour of Ψ_h at $t = 3000\tau_A$ (left) and $t = 3800\tau_A$ (right) for $r \leq 0.8$. Dashed lines show the position of the surfaces with $\iota_T = 1/2$.

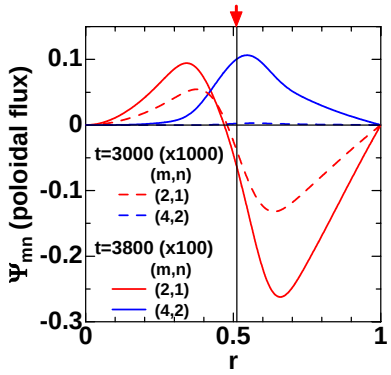

Fig.4. Profiles of perturbed poloidal flux. Red arrow indicates the position of $\iota_{eq} = 1/2$.

neous islands ($\theta = 0$ and $\theta = \pi$) , as shown in Fig.3(right). We call them minor X-points. As a result, the $m = 4$ islands exist inside the $m = 2$ islands. This island structure corresponds to the mode structure of $\tilde{\Psi}_{mn}$ shown in Fig.4. The component of $\tilde{\Psi}_{42}$, which is an even function, has a comparable value with that of $\tilde{\Psi}_{21}$ at the resonant surface.

The appearance of the even function of $\tilde{\Psi}_{42}$ can be explained analytically. For simplicity, we employ the slab geometry around the resonant surface, $r = r_s$. We introduce an ordering that the Fourier components $\tilde{\Phi}_{mn}(x)$ and $\tilde{\Psi}_{mn}(x)$ should be the order of $O(\delta^n)$ with small parameter δ, where $x = r - r_s$. The lowest order of $\tilde{\Phi}_{mn}$ is $\tilde{\Phi}_{21}$ in $O(\delta)$. As the structure of the mode can be approximated by the linear eigenfunction, $\tilde{\Phi}_{21}$ can be written as $\tilde{\Phi}_{21} = \overline{\Phi}\exp[-x^2/(2w_{21}^2)]$, where $\overline{\Phi}$ is a constant and w_{21} denotes the mode width. Then, the function of $\tilde{\Psi}_{21}$ can be obtained from the Ohm's law in the order of $O(\delta)$. By substituting $\tilde{\Phi}_{21}$ and $\tilde{\Psi}_{21}$ into the Ohm's law in the next order, we can obtain the function of $\tilde{\Psi}_{42}$, which are given by $\tilde{\Psi}_{42} = \overline{\Psi}\{1 + (A/S)[4 - 5(x^2/w_{21}^2)]\}\exp[-x^2/(w_{21}^2)]$. Here $\overline{\Psi}$ and A are constant. The resistive term is included successively up to $O(1/S)$ here. The expression of $\tilde{\Psi}_{42}$ shows an even function with the width of $w_{21}/\sqrt{2}$, which corresponds to the structure shown in Fig.4.

The mechanism of the minor X-point generation can be explained with the change of the radial magnetic component $\tilde{B}_r$. To change O-point to X-point with the poloidal component of the helical magnetic field fixed, the direction of $\tilde{B}_r$ has to be reversed around the point. This is shown in Fig.5 where we have plotted $\tilde{B}_r$ along the resonant surface in the poloidal cross section. In the region of $0 \leq \theta \leq 0.2\pi$, $\tilde{B}_r$ is negative for $t \leq 3500\tau_A$ while it is positive for $t \geq 3600\tau_A$ in the present case.

The perturbed magnetic field vector is tangential to the surface of $\tilde{\Psi} = const$. Hence, the reversal of B_r direction is concerned with the structure of the $\tilde{\Psi} = const$. surface. Figure 6

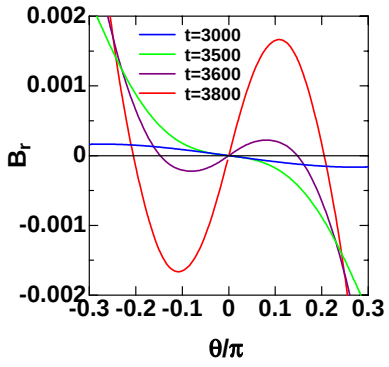

Fig.5. Time evolution of $\tilde{B}_r$ profile along the resonant surface.

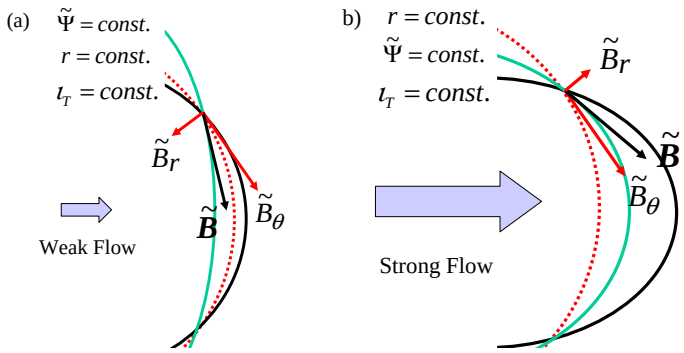

Fig.6. Schematic pictures of $\tilde{\Psi}$ around $\theta = 0$ at (a) $t = 3000\tau_A$ and (b) $t = 3800\tau_A$.

schematically shows the surfaces of $\tilde{\Psi} = const.$, $r = const.$ and $\iota_T = 1/2$ on the $z = 0$ poloidal cross section, which cross at $\theta = 0.1\pi$. The numerical result shows that the radial curvature of the $\tilde{\Psi} = const.$ surface is smaller than $1/r$ at $t = 3000\tau_A$. This indicates that $\tilde{B}_r$ is negative at the cross point as shown in Fig.6(a). On the other hand, at $t = 3800\tau_A$, the radial curvature of the $\tilde{\Psi} = const.$ surface is larger than $1/r$ at the same position. This indicates that $\tilde{B}_r$ is positive. Therefore, the curvature enhancement of the $\tilde{\Psi} = const.$ surface results in the generation of the minor X-point. This curvature enhancement is caused by the increase of the outward radial flow shown in Fig.2.

4. Conclusions

In the nonlinear saturation phase of the resistive interchange mode, magnetic islands can be generated by the flow across the resonant surface. In this case, the poloidal number of the island is twice that of the poloidal mode number of the dominant component. The curvature enhancement of the perturbed poloidal flux contour due to the increase of the radial flow is essential in the reconnection process. This mechanism is different from that of the standard driven reconnection because current concentration at the resonant surface is not observed.

Acknowledgments

This work was partially supported by the Grant-in-Aid for Scientific Research (C) 13680572 of Japan Society for the Promotion of Science.

References

[1] M.Wakatani, et al., Nucl. Fusion **24** (1984) 1407.

[2] B.A.Carreras, et al., Phys. Plasmas **10** (1998) 3700.

[3] K.Ichiguchi, et al., Nucl. Fusion **43** (2003) 1101.